[10]G. Wolf, Nucl. Phys. B26, 317 (1971).
[10a]C. Berger, N. Mistry, L. Roberts, T. Talman, and P. Walstrom, Cornell Report No. CLNS-168, 1971 (unpublished).
[11]H. Bingham *et al.*, Phys. Rev. Letters 24, 955 (1970).
[12]H. Alvensleben *et al.*, Phys. Rev. Letters 23, 1058 (1969).
[13]R. L. Anderson *et al.*, Phys. Rev. D 1, 27 (1970).
[14]M. Damashek and F. Gilman, Phys. Rev. D 1, 1319 (1970).
[15]J. Trefil, Phys. Rev. 180, 1366 (1969); 180, 1379 (1969).
[16]R. L. Anderson *et al.*, paper submitted to the Fifteenth International Conference on High-Energy Physics, Kiev, U.S.S.R., 1970 (unpublished); see rapporteur talk by K. Lübelsmeyer, in *Proceedings of the Fifteenth International Conference on High-Energy Physics, Kiev, U.S.S.R., 1970* (Atomizdat, Moscow, 1971).
[17]H. Alvensleben *et al.*, Phys. Rev. Letters 24, 786 (1970).

PHYSICAL REVIEW D VOLUME 4, NUMBER 9 1 NOVEMBER 1971

Experimental Results on the Reactions $\pi^- p \to \pi\pi N$ in the c.m. Energy Range 1400–2000 MeV*

A. D. Brody,† R. J. Cashmore, A. Kernan,‡ D. W. G. S. Leith, B. G. Levi, A. Minten,† and B. C. Shen‡
Stanford Linear Accelerator Center, Stanford University, Stanford, California 94305

and

J. P. Berge,† B. Deler,§ D. J. Herndon, R. Longacre, L. R. Miller, L. R. Price,|| A. H. Rosenfeld, and P. Söding**
Lawrence Radiation Laboratory, University of California, Berkeley, California 94720
(Received 12 July 1971)

Cross sections and representative distributions are given for the reactions $\pi^- p \to \pi^+\pi^- n$, $\pi^- p \to \pi^- p\pi^0$ based on 85 000 inelastic events in the c.m. energy region 1400–2000 MeV. The angular distributions of beam, defined with respect to the final-state particles are given in terms of their moments as a function of Dalitz plot position and c.m. energy.

I. INTRODUCTION

Although the elastic and charge-exchange channels of pion-nucleon scattering experiments have been studied extensively,[1-8] the data on inelastic channels remain incomplete.[9] These channels are becoming more important since the phase-shift analyses, which have been successful in revealing the major features of the πN system, are in considerable disagreement over the detailed features of partial waves of low elasticity. For these reasons we have made systematic measurements of inelastic channels in the energy region 1400–2000 MeV.

The origin of these data are exposures of the 72-in. hydrogen bubble chamber (HBC) at Lawrence Radiation Laboratory, Berkeley, and the 30-in. HBC at Argonne National Laboratory to π^- beams in the momentum range 550–1600 MeV/c. This paper is concerned with the study of inelastic two-prong events observed in this film, i.e.,

$$\pi^- p \to \pi^+\pi^- n, \quad \sim 51\,000 \text{ events}; \tag{1}$$

$$\pi^- p \to \pi^-\pi^0 p, \quad \sim 34\,000 \text{ events}. \tag{2}$$

The other major contribution to the two-prong topology comes from elastic scattering

$$\pi^- p \to \pi^- p, \quad \sim 80\,000 \text{ events} \tag{3}$$

and this has been discussed previously.[10]

Within three c.m. energy regions, 1400–1600, 1600–1800, and 1800–2000 MeV, our data correspond to approximate μb equivalents of 0.5, 2.0, and 2.5 events per μb, respectively.

In Sec. II we describe the identification of events from reactions (1) and (2) and other details of the data analysis. In Sec. III we give cross sections for these two channels and in Sec. IV we describe the general characteristics of the reactions and give the results of moments analysis of reactions (1) and (2) throughout our entire c.m. energy region. Section V contains the results of an analysis of the $\pi^+\pi^- n$ final state leading to a presentation of the $\Delta\pi$ and ρN partial cross sections. The results of an analysis of the $\Delta^-\pi^+$ final state over a limited energy range are also summarized. Section VI contains only a short discussion of the results. The main purpose of this paper is a presentation of the experimental results. A detailed discussion of the partial-wave analyses of the inelastic data now in progress will appear at a later date.

II. DATA ANALYSIS

Details of the beams, experimental procedures, scanning and measuring, and data reduction have been described previously.[10] The film was scanned for all two-prong events which were then subsequently measured on an LRL Spiral Reader. In this section we are only concerned with the identification of reactions (1) and (2).

An attempt is made to fit all two-prong events with the hypotheses corresponding to reactions (1)–(3). Because the elastic scattering (3) is more highly constrained than the remaining one-constraint hypotheses, all events that satisfy this hypothesis with a χ^2 for the kinematic fit, χ_K^2, less than 25 were accepted as elastic scatters.

If an event satisfied either (1) or (2) only, with a value of χ_K^2 less than a prescriped value ($\chi_K^2 = 7$ for the Argonne film and $\chi_K^2 = 8$ for the Berkeley film) then that hypothesis was unambiguously selected. However, if an event satisfied both of these hypotheses, we adopt certain criteria to select the "best" fit. [In the Argonne film ~15% of inelastic events were ambiguous between the two interpretations (1) and (2) after just kinematical fitting. The corresponding number for the Berkeley film was ~18%.] We considered not only the χ_K^2 for the kinematic fit but also the χ_{ion}^2 for the fit of the calculated ionization to that determined experimentally from pulse-height measurements of the Spiral Reader. At the relatively low energies involved in the present experiment, the difference in ioniza-

TABLE I. Events processed at each energy.

Exposure	$E_{\text{c.m.}}$ (MeV)	$p_{\text{lab}}^{\pi^-}$ (MeV/c)	4-C events $\chi^2 \leq 14$	1-C $n\pi\pi$ events $\chi^2 \leq 8$	1-C $p\pi\pi$ events $\chi^2 \leq 8$
30-in. HBC I	1406	556	648	255	80
	1440	609	500	215	82
	1472	660	1110	418	245
	1496	699	1854	675	499
	1527	750	2337	832	701
	1556	797	826	340	272
	1589	853	997	579	387
	1709	1067	1141	585	400
	1730	1105	1954	1046	836
	1762	1165	2230	1231	899
30-in. HBC II	1811	1259	1544	1096	651
	1843	1322	2777	2172	1337
	1872	1381	2920	2443	1568
	1904	1444	3160	2616	1694
	1935	1509	1606	1288	886
30-in. HBC II	1720	1084	687	392	262
	1761	1161	1200	786	488
	1787	1212	1210	798	476
	1806	1250	292	188	122
	1821	1278	1740	1098	687
	1853	1340	2213	1649	979
	1885	1404	2392	1970	1180
	1916	1469	3792	3203	2105
	1933	1503	1972	1735	1177
	1963	1567	4113	3512	2405
	1980	1602	3957	3416	2458
				$\chi^2 \leq 7$	$\chi^2 \leq 7$
72-in. HBC	1628	924	537	358	200
	1647	956	5482	3169	1968
	1660	979	2697	1430	879
	1669	995	5127	2562	1603
	1674	1004	4966	2673	1568
	1685	1024	4398	2281	1409
	1695	1042	2206	1299	871
	1740	1125	3594	2259	1786
	1766	1174	1733	1120	854
Totals			79 911	51 477	33 880

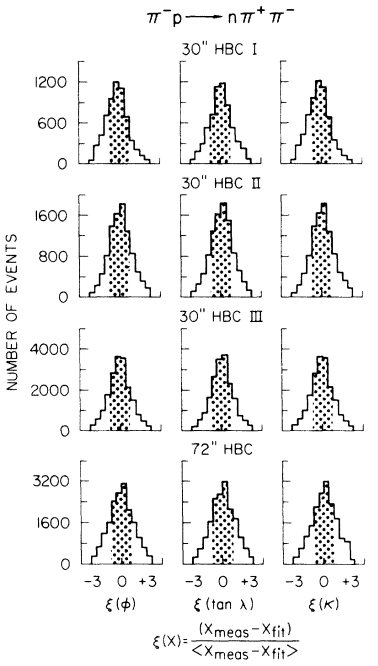

FIG. 1. Beam-track pull quantities in the reaction $\pi^- p \to \pi^-\pi^+ n$. The shaded area corresponds to ±1. For definitions of HBC I, HBC II, and HBC III, see Table I.

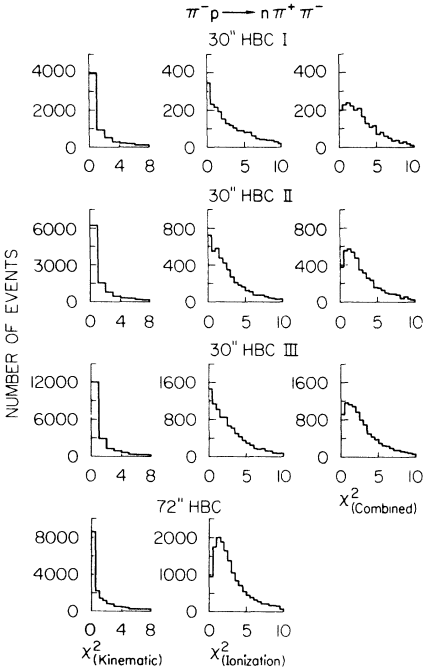

FIG. 3. χ^2 distributions for the reaction $\pi^- p \to \pi^-\pi^+ n$. The value of $\chi_{comb}{}^2$ is discussed in Sec. II. For definitions of HBC I, HBC II, and HBC III, see Table I.

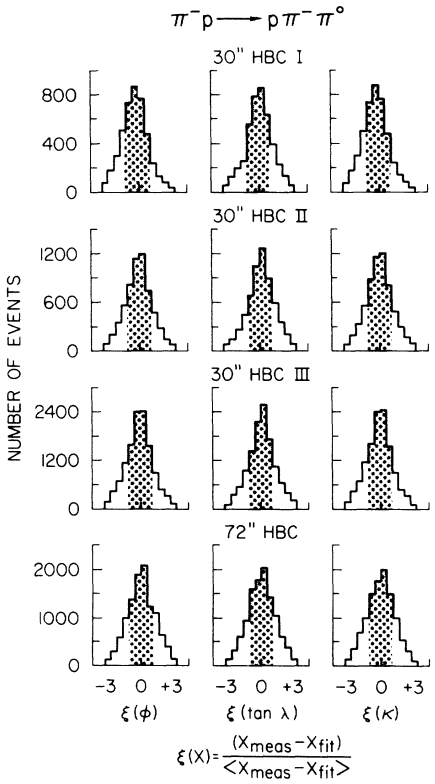

FIG. 2. Beam-track pull quantities in the reaction $\pi^- p \to \pi^-\pi^0 p$. The shaded area corresponds to ±1. For definitions of HBC I, HBC II, and HBC III, see Table I.

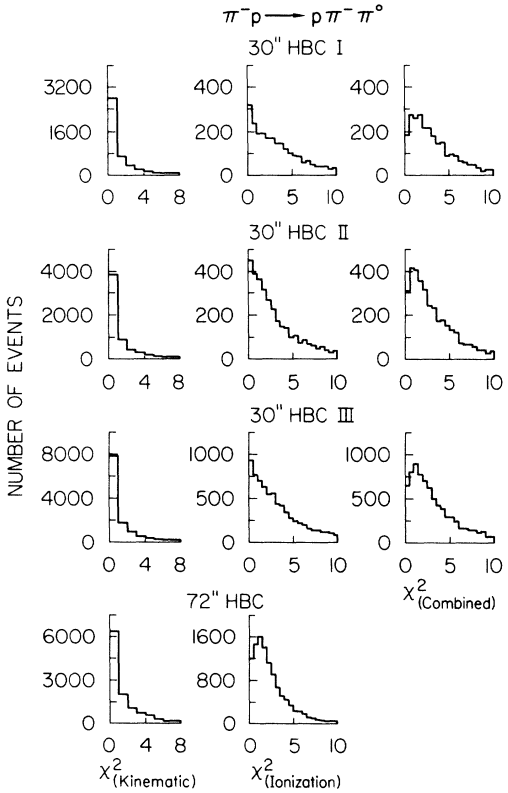

FIG. 4. χ^2 distributions for the reaction $\pi^- p \to \pi^-\pi^0 p$. The value of $\chi_{comb}{}^2$ is discussed in Sec. II. For definitions of HBC I, HBC II, and HBC III, see Table I.

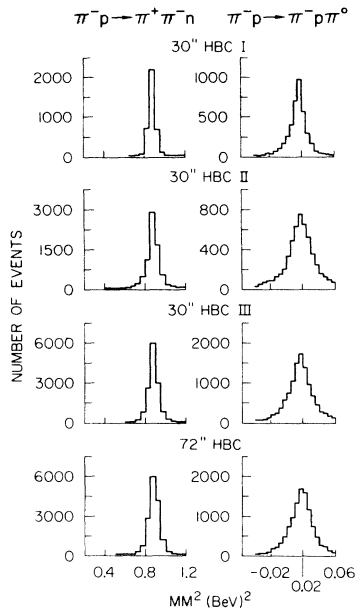

FIG. 5. Missing-mass distributions for the reactions $\pi^-p\to\pi^-\pi^+n$ and $\pi^-p\to\pi^-\pi^0p$. For definitions of HBC I, HBC II, and HBC III, see Table I.

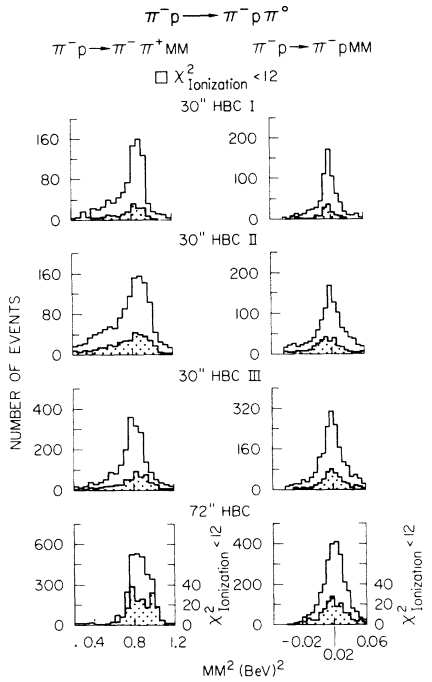

FIG. 7. Missing-mass distributions for ambiguous events assigned to the reaction $\pi^-p\to\pi^-\pi^0p$. For definitions of HBC I, HBC II, and HBC III, see Table I.

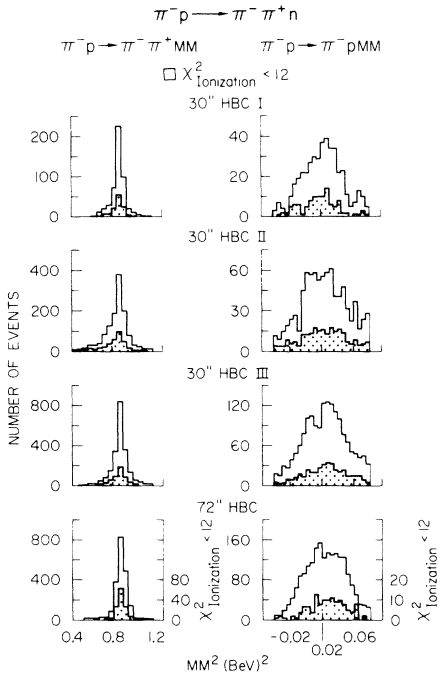

FIG. 6. Missing-mass distributions for ambiguous events assigned to the reaction $\pi^-p\to\pi^-\pi^+n$. For definitions of HBC I, HBC II, and HBC III, see Table I.

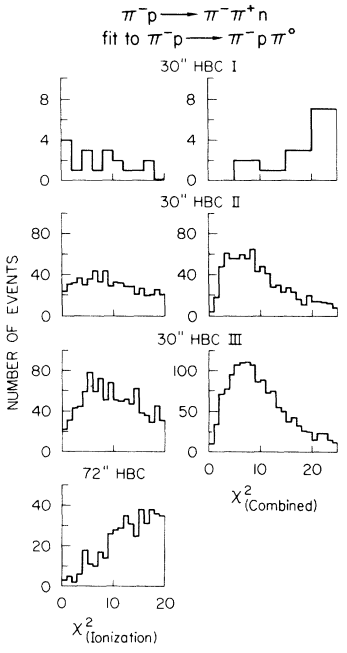

FIG. 8. χ^2 distribution for ambiguous events assigned to the reaction $\pi^-p\to\pi^-\pi^+n$ when interpreted as being $\pi^-p\to\pi^-\pi^0p$. For definitions of HBC I, HBC II, and HBC III, see Table I.

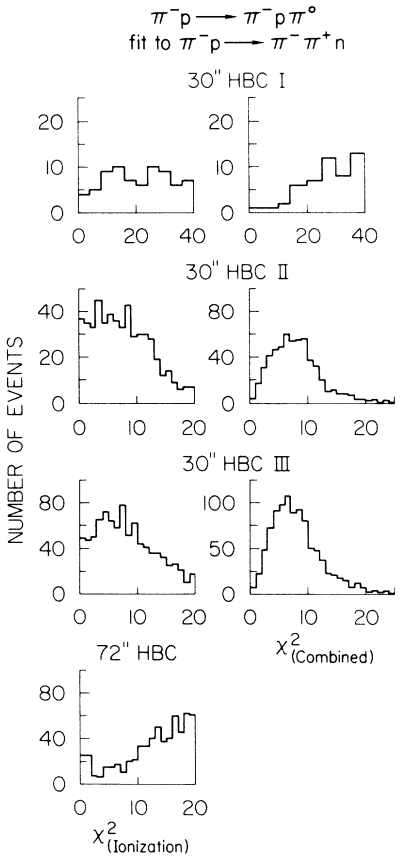

FIG. 9. χ^2 distribution for ambiguous events assigned to the reaction $\pi^- p \to \pi^- \pi^0 p$ when interpreted as being $\pi^- p \to \pi^- \pi^+ n$. For definitions of HBC I, HBC II, and HBC III, see Table I.

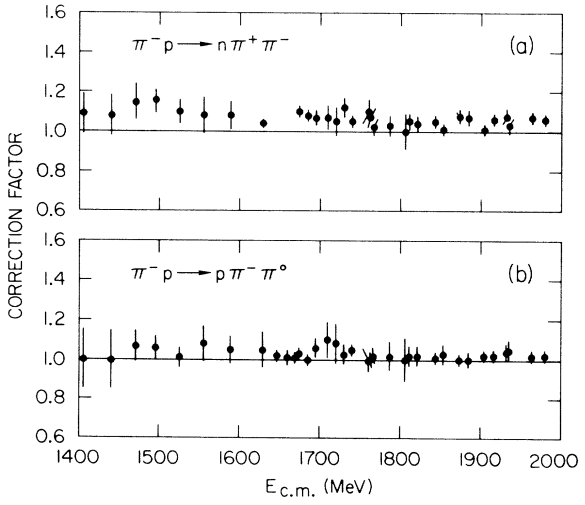

FIG. 10. (a) Azimuthal correction factors as a function of c.m. energy for the reaction $\pi^- p \to \pi^- \pi^+ n$. (b) Azimuthal correction factors as a function of c.m. energy for the reaction $\pi^- p \to \pi^- \pi^0 p$. The numerical values for these quantities are given in Table II.

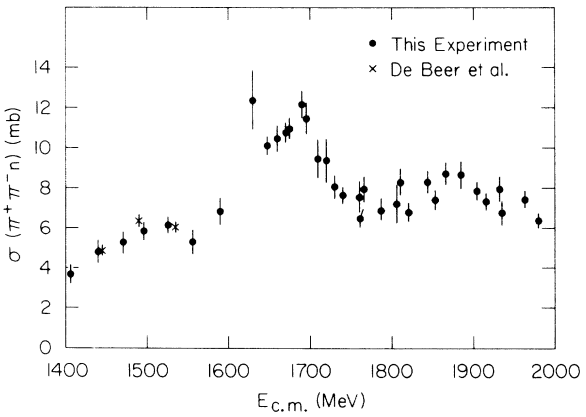

FIG. 11. Cross sections for the reaction $\pi^- p \to \pi^- \pi^+ n$.

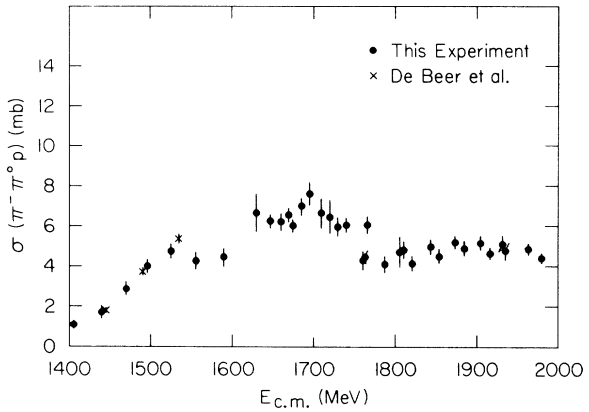

FIG. 12. Cross sections for the reaction $\pi^- p \to \pi^- \pi^0 p$.

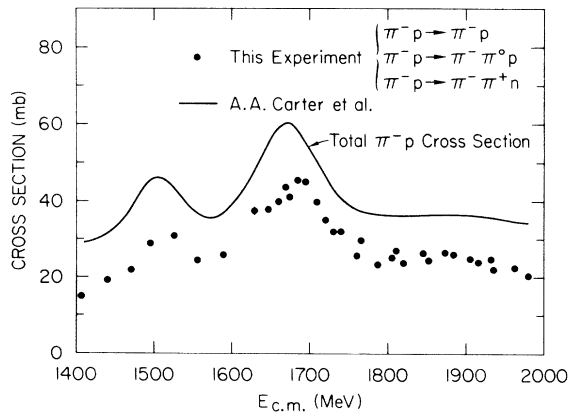

FIG. 13. Cross section for the reactions $\pi^- p \to \pi^- p$, $\pi^- p \to \pi^- \pi^+ n$, and $\pi^- p \to \pi^- \pi^0 p$, compared with the total cross-section measurements of Carter *et al.*[11]

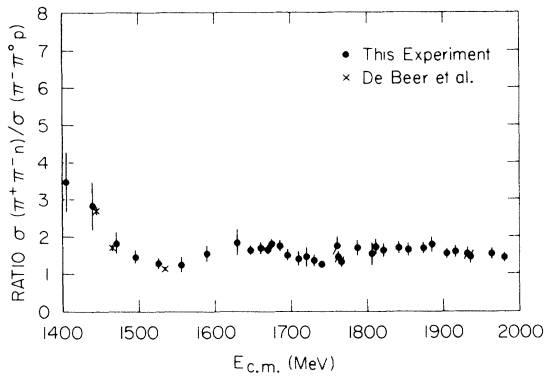

FIG. 14. Ratio $\sigma(\pi^+\pi^-n)/\sigma(\pi^-\pi^0p)$ as a function of energy.

TABLE II. Azimuthal correction factors and errors.

$E_{c.m.}$ (MeV)	$\pi^+\pi^-n$ Correction	$\pi^+\pi^-n$ Error	$\pi^-\pi^0p$ Correction	$\pi^-\pi^0p$ Error
1406	1.09	0.10	1.00	0.15
1440	1.08	0.10	1.00	0.15
1471	1.15	0.09	1.07	0.08
1496	1.15	0.06	1.06	0.06
1527	1.10	0.06	1.01	0.05
1556	1.08	0.09	1.08	0.09
1589	1.08	0.07	1.05	0.07
1629	1.09	0.07	1.05	0.09
1647	1.03	0.02	1.02	0.03
1660	1.05	0.03	1.01	0.04
1669	1.04	0.02	1.01	0.03
1674	1.10	0.03	1.03	0.03
1685	1.08	0.03	1.00	0.03
1695	1.07	0.04	1.06	0.05
1709	1.07	0.06	1.10	0.09
1720	1.05	0.07	1.08	0.10
1730	1.12	0.05	1.03	0.05
1740	1.05	0.03	1.05	0.03
1761	1.10	0.06	1.00	0.06
1762	1.07	0.05	1.00	0.04
1766	1.02	0.04	1.02	0.04
1787	1.03	0.05	1.02	0.07
1806	1.00	0.09	1.00	0.11
1811	1.05	0.04	1.02	0.05
1821	1.04	0.04	1.02	0.05
1843	1.05	0.03	1.01	0.03
1853	1.01	0.03	1.03	0.05
1873	1.08	0.04	1.00	0.03
1884	1.07	0.04	1.00	0.04
1904	1.01	0.03	1.02	0.03
1916	1.06	0.03	1.02	0.03
1932	1.08	0.04	1.04	0.04
1935	1.03	0.04	1.05	0.05
1963	1.07	0.03	1.02	0.03
1980	1.06	0.03	1.02	0.03

tion between a proton and a pion track can often be decisive. For the 72-in. Alvarez HBC film we used the following selection criteria:

(a) We chose that hypothesis which gave the lower value of the χ_{ion}^2, provided the difference was larger than 3,

(b) If the difference in χ_{ion}^2 for the two fits was less than 3, we chose that hypothesis which gave the lower value of χ_K^2, providing this difference was larger than 1.5.

(c) If the difference in χ_K^2 was also less than 1.5, we selected that hypothesis which gave the lower value of χ_{ion}^2.

For the 30-in. MURA (Midwest Universities Research Association) HBC film, we employed a simpler selection criterion. We formed a linear combination of χ_K^2 and χ_{ion}^2, which is called the combined χ^2 or χ_{comb}^2.[11] We assigned an ambiguous event to either reaction (1) or (2) depending on which fit gave the lower value of χ_{comb}^2. To compare the results of the two selection procedures, we made the selection in both manners for a sample of events. The resulting identifications were esentially identical.

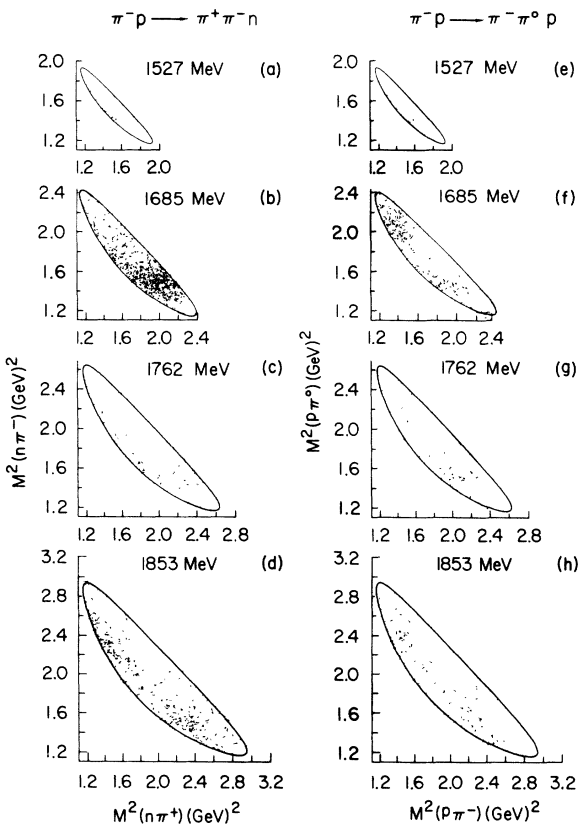

FIG. 15. Dalitz plots for the reactions $\pi^-p \to \pi^-\pi^+n$, $\pi^-p \to \pi^-\pi^0p$.

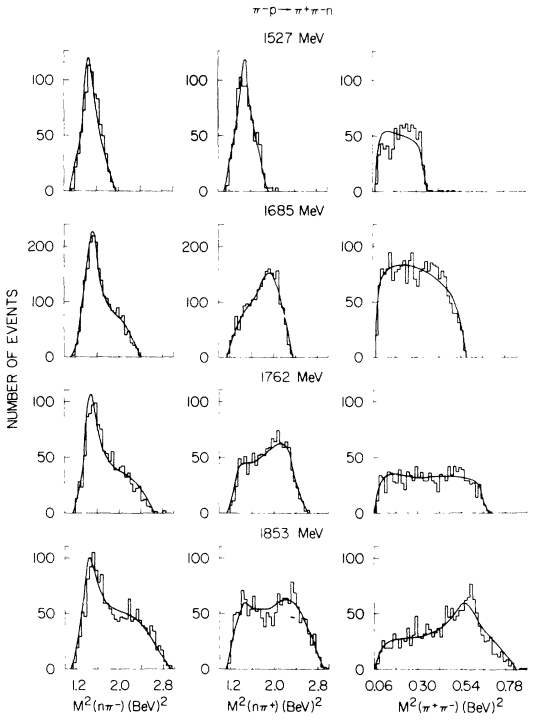

FIG. 16. Mass-squared projections of the Dalitz plot in the final state $\pi^- p \to \pi^-\pi^+ n$. The curves are from maximum-likelihood fits to the Dalitz plot described in Sec. V.

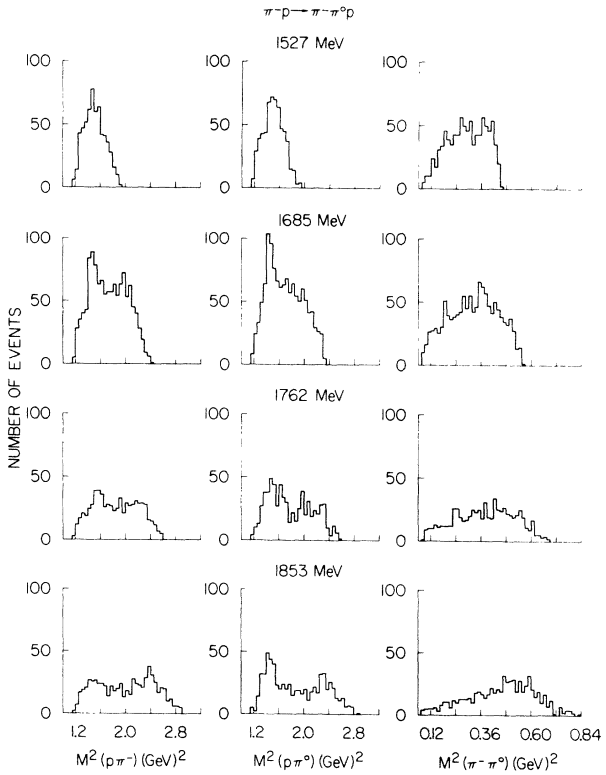

FIG. 17. Mass-squared projections of the Dalitz plot in the final state $\pi^- p \to \pi^-\pi^0 p$.

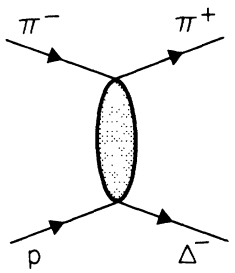

FIG. 18. Diagram for the production of forward π^+ mesons in the reaction $\pi^- p \to \pi^+ \Delta^-$.

In Figs. 1 and 2 we present the pull quantities for the beam track, shown separately for the four-experimental runs that comprise the experiment and the two reactions (1) and(2). In Figs. 3 and 4 we plot the χ^2 values χ_K^2, χ_{ion}^2, and χ_{comb}^2, while in Fig. 5 we show the missing mass squared of the missing particle in events assigned to reactions (1) and (2).

In order to study whether the ambiguities have been correctly resolved, we examine several quantities corresponding to the "wrong" hypothesis in the sample of ambiguous events. Figures 6 and 7 display the missing mass squared for both the "right" and "wrong" interpretations. The distributions for the "wrong" choice appear far too broad, especially in comparison with the corresponding plot for the "right" choice. The shaded histograms correspond to the samples of these events with χ_{ion}^2 less than 12 for the "wrong" hypothesis. The dis-

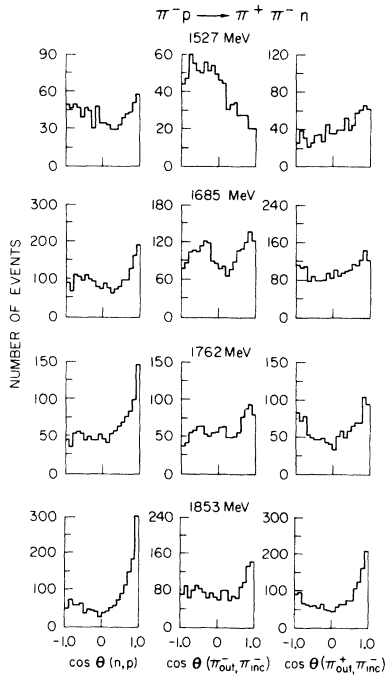

FIG. 19. Production angular distributions of each particle in the final state $\pi^- p \to \pi^+\pi^- n$.

tributions are not improved by this cut and thus none of these events are examples of the reaction corresponding to the "wrong" choice. In Figs. 8 and 9 we show the χ_{ion}^2 and χ_{comb}^2 distributions corresponding to the "wrong" choice. They do not display the correct characteristics of two- and three-constraint fits. From these observations we have concluded that the selection criteria we have adopted are reasonable and introduce negligible contamination in the total sample of events.

After the events were measured, processed, and separated according to the reaction type, we obtained a total of ~51 000 events in the final states $\pi^+\pi^-n$ and ~34 000 events in the final state $\pi^-\pi^0p$. The statistics, broken down by energy regions, are given in Table I. The energy is the central value determined from the corresponding sample of elastic scatters. We chose to use these values because of the higher statistics and smaller errors in this final state together with the fact that we used the elastic data for normalization in obtaining the cross sections.[10]

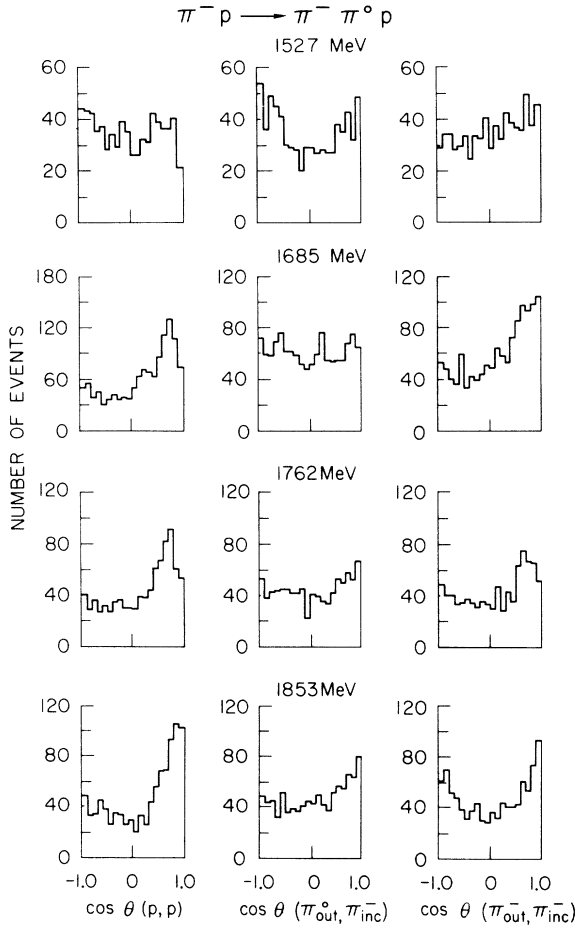

FIG. 20. Production angular distributions of each particle in the final state $\pi^-p \to \pi^-\pi^0p$.

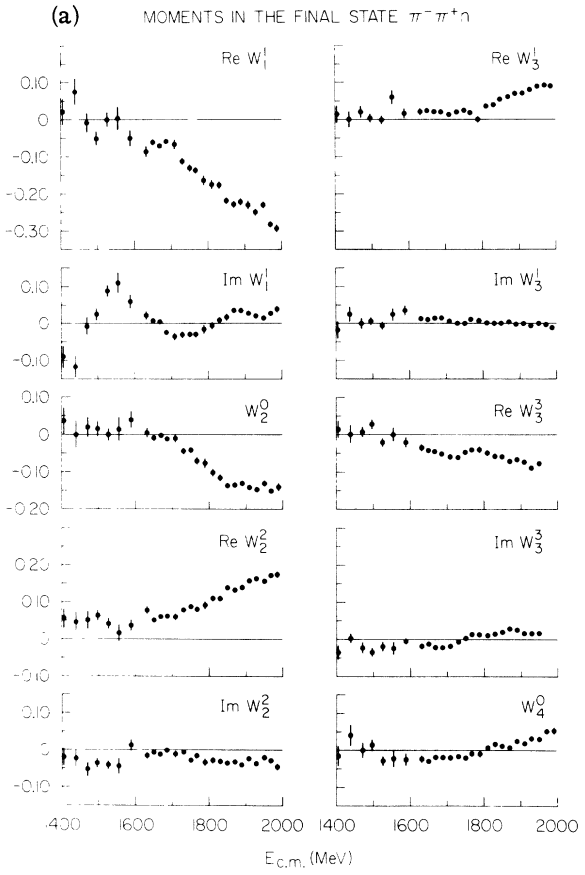

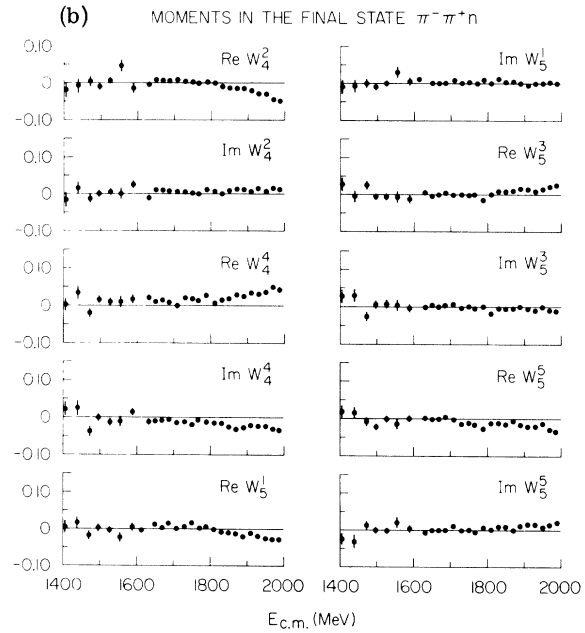

FIG. 21. (a) and (b) The moments W_L^M as a function of energy in the final state $\pi^-\pi^+n$ normalized such that $W_0^0 = 1$ [see Eq. (4′)]. The x axis is defined as $\vec{P}_n$, and the z axis as $\vec{P}_{\pi^-} \times \vec{P}_{\pi^+}$.

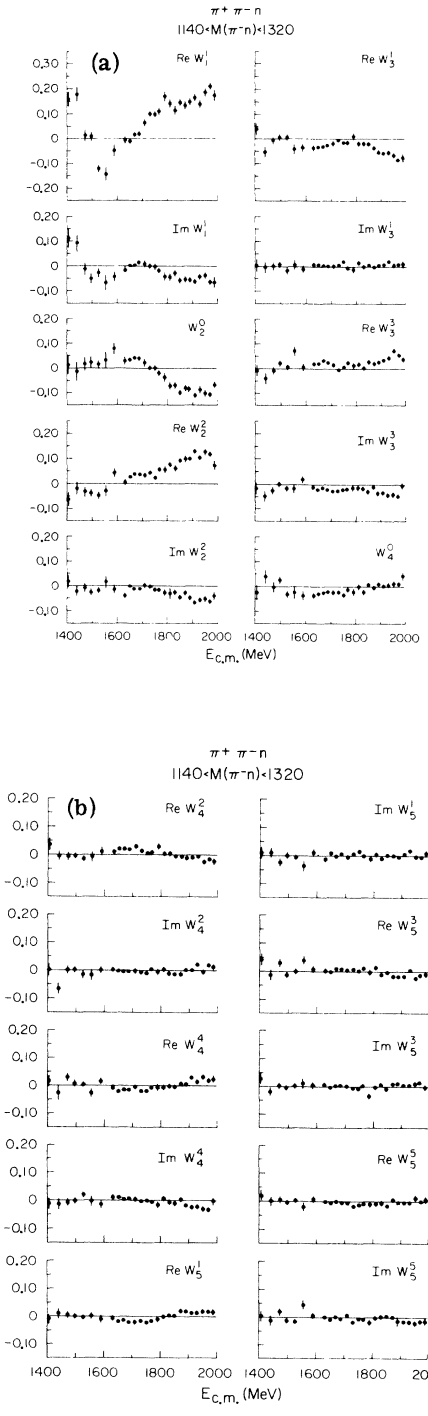

FIG. 22. (a) and (b) The moments W_L^M as a function of energy in the final state $\pi^-\pi^+n$ for $1140 < M(\pi^-n) < 1320$ MeV normalized such that $W_0^0 = 1$ [see Eq. (4′)]. The x axis is defined as $\vec{P}_{\pi^+}$ and the z axis as $\vec{P}_{\pi^-} \times \vec{P}_{\pi^+}$.

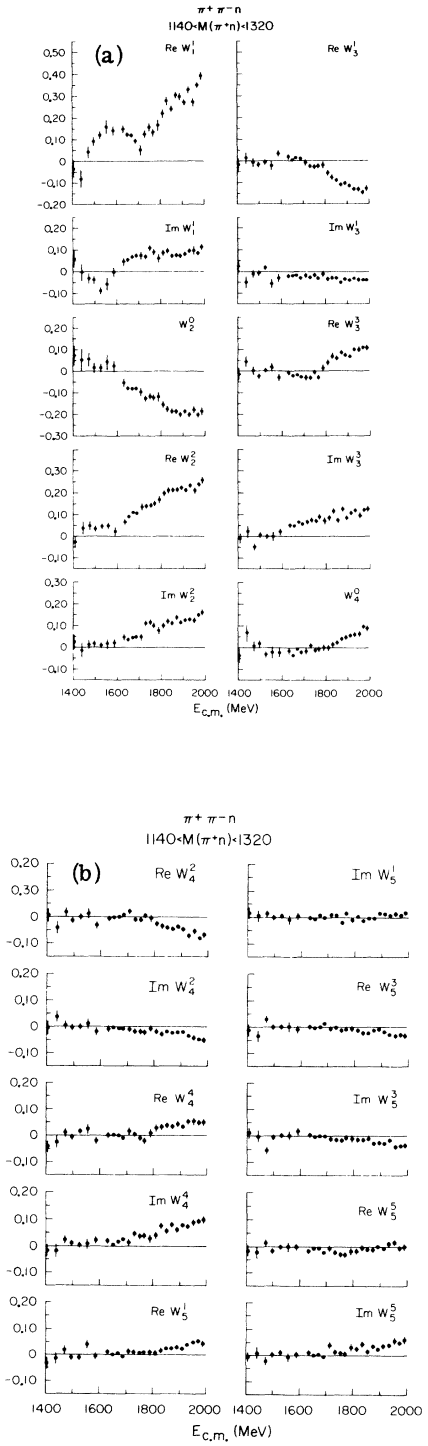

FIG. 23. (a) and (b) The moments W_L^M as a function of energy in the final state $\pi^-\pi^+n$ for $1140 < M(\pi^+n) < 1320$ MeV normalized such that $W_0^0 = 1$ [see Eq. (4′)]. The x axis is defined as $\vec{P}_{\pi^-}$ and the z axis as $\vec{P}_{\pi^-} \times \vec{P}_{\pi^+}$.

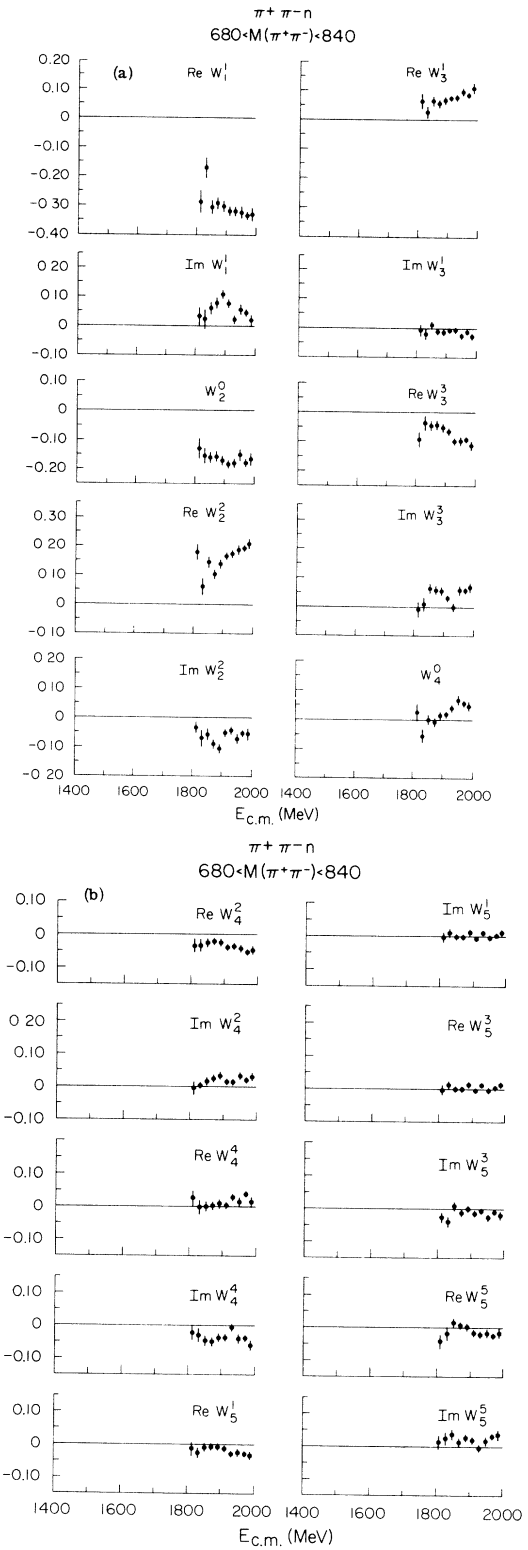

FIG. 24. (a) and (b) The moments W_L^M as a function of energy in the final state $\pi^-\pi^+n$ for $680 < M(\pi^-\pi^+) < 840$ MeV normalized such that $W_0^0 = 1$ [see Eq. (4′)]. The x axis is defined as $\vec{P}_n$ and the z axis as $\vec{P}_{\pi^-} \times \vec{P}_{\pi^+}$.

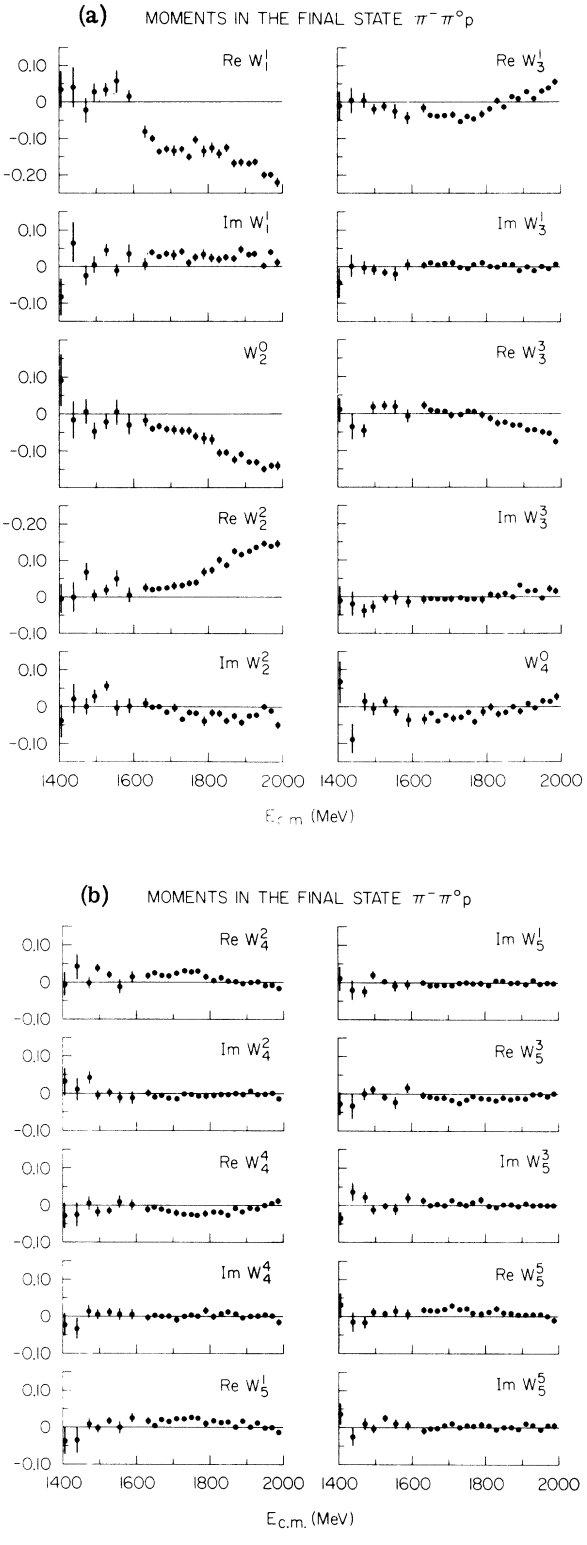

FIG. 25. (a) and (b) The moments W_L^M as a function of energy in the final state $\pi^-\pi^0p$ normalized such that $W_0^0 = 1$ [see Eq. (4′)]. The x axis is defined as $\vec{P}_p$ and the z axis as $\vec{P}_{\pi^-} \times \vec{P}_{\pi^0}$.

III. CROSS SECTIONS

In determining the total elastic cross section we used a procedure of normalizing our data in a limited range of the angular distribution to counter measurements in the same region, after the necessary corrections had been made.[10] This then gives the cross section per event for the various energy regions of our film, both for the elastic and inelastic reactions. This procedure would be unsatisfactory if elastic events are fitted and accepted more efficiently than inelastic events. No evidence of this exists, the proportions of elastic and inelastic events being the same in both the first measurements of the data and the subsequent measurements of those events which initially failed.

In the case of the inelastic data we again investigated the distribution of events about the beam direction. We define a normal to the plane of the two outgoing tracks and look at the azimuthal distribution of this normal using a coordinate system in which the camera axis is defined to be the x axis and the beam direction the z axis. A small loss of events is observed when the normal is perpendicular to the camera axis. The corrections for this effect are given in Table II and Fig. 10.

After making these corrections the cross sections for the two inelastic reactions are given in Table III, together with the total elastic cross section at the same energy.[10] Figures 11 and 12 display these inelastic cross sections while in Fig. 13 we compare the total cross section of Carter *et al.*,[12]

TABLE III. Cross sections.

$E_{c.m.}$ (MeV)	$\pi^- p \to \pi^- p$		$\pi^- p \to \pi^- \pi^+ n$		$\pi^- p \to \pi^- \pi^0 p$	
	σ (mb)	$\delta\sigma$ (mb)	σ (mb)	$\delta\sigma$ (mb)	σ (mb)	$\delta\sigma$ (mb)
1406	10.24	0.62	3.67	0.46	1.06	0.21
1440	12.86	0.94	4.79	0.62	1.69	0.33
1471	15.32	0.80	5.25	0.55	2.86	0.32
1496	19.07	0.74	5.84	0.47	3.98	0.35
1527	19.91	0.71	6.12	0.47	4.74	0.35
1556	14.91	0.96	5.30	0.60	4.24	0.49
1589	14.47	0.84	6.83	0.64	4.44	0.44
1629	18.80	1.32	12.38	1.47	6.66	0.93
1647	21.62	0.46	10.10	0.47	6.21	0.33
1660	23.16	0.66	10.47	0.64	6.19	0.43
1669	26.42	0.58	10.76	0.50	6.54	0.35
1674	24.22	0.54	10.92	0.54	6.00	0.32
1685	26.30	0.75	12.17	0.69	6.96	0.42
1695	26.01	0.86	11.45	0.77	7.60	0.58
1709	23.65	1.10	9.46	0.83	6.65	0.73
1720	19.48	1.35	9.33	1.06	6.41	0.87
1730	17.95	0.74	8.07	0.59	5.93	0.46
1740	18.29	0.47	7.64	0.40	6.04	0.32
1761	13.66	0.78	7.56	0.74	4.26	0.45
1762	15.01	0.50	6.49	0.47	4.43	0.31
1766	15.73	0.61	7.95	0.61	6.06	0.47
1787	12.45	0.59	6.92	0.55	4.09	0.40
1806	13.31	1.08	7.22	0.98	4.68	0.75
1811	13.80	0.61	8.30	0.64	4.79	0.41
1821	12.80	0.55	6.76	0.47	4.15	0.33
1843	13.09	0.45	8.33	0.54	4.93	0.34
1853	12.38	0.45	7.40	0.50	4.48	0.36
1873	12.53	0.39	8.73	0.55	5.19	0.32
1884	12.34	0.50	8.68	0.67	4.86	0.39
1904	11.95	0.36	7.84	0.47	5.13	0.31
1916	10.87	0.36	7.31	0.45	4.62	0.30
1932	11.69	0.49	7.97	0.61	5.21	0.41
1935	10.39	0.47	6.76	0.58	4.74	0.44
1963	10.21	0.29	7.43	0.42	4.85	0.28
1980	9.82	0.33	6.36	0.36	4.40	0.26

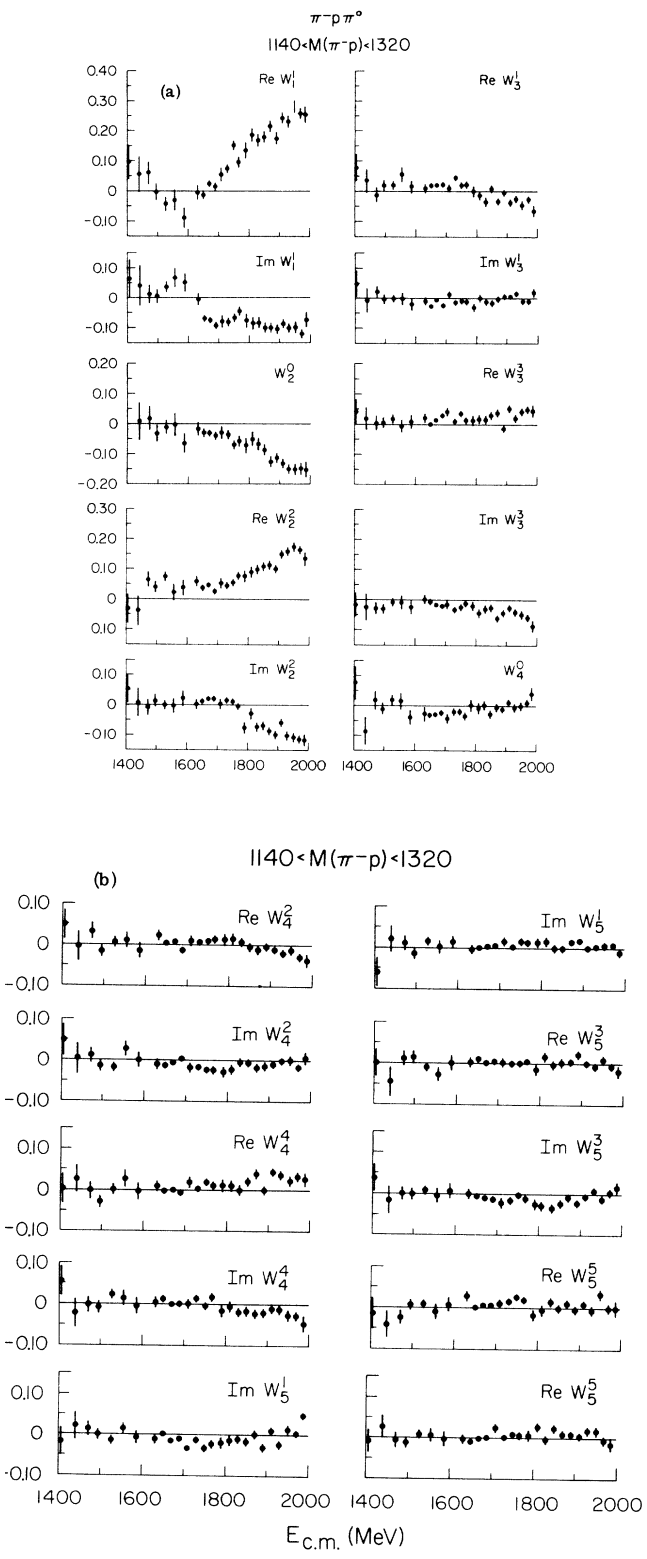

FIG. 26. (a) and (b) The moments W_L^M as a function of energy in the final state $\pi^-\pi^0 p$ for $1140 < M(\pi^- p) < 1320$ MeV normalized such that $W_0^0 = 1$ [see Eq. (4′)]. The x axis is defined as $\vec{P}_{\pi^0}$ and the z axis as $\vec{P}_{\pi^-} \times \vec{P}_{\pi^0}$.

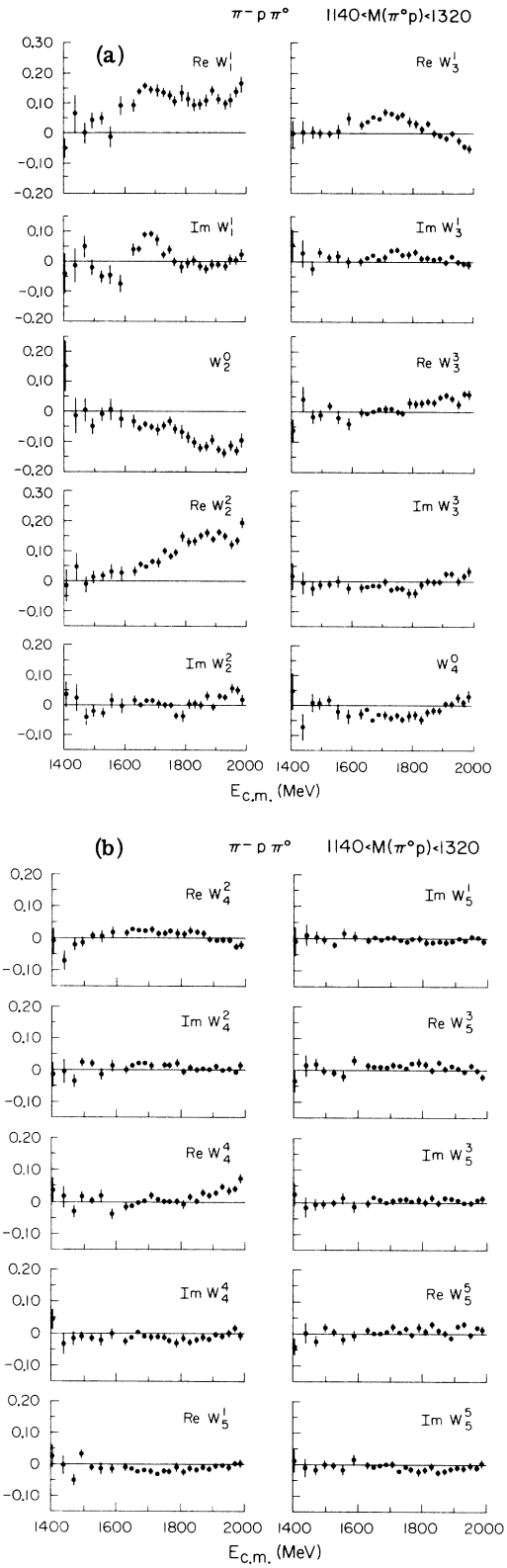

FIG. 27. (a) and (b) The moments W_L^M as a function of energy in the final state $\pi^-\pi^0 p$ for $1140 < M(\pi^0 p) < 1320$ MeV normalized such that $W_0^0 = 1$ [see Eq. (4′)]. The x axis is defined as $\vec{P}_{\pi^-}$ and the z axis as $\vec{P}_{\pi^-} \times \vec{P}_{\pi^0}$.

with the cross section for reactions (1), (2), and (3). In Fig. 14 we give the ratio of the cross sections for production of the $\pi^+\pi^- n$ and $\pi^- p\pi^0$ final states as a function of energy. In these graphs we also include other measurements of the inelastic reactions.[13]

IV. EXPERIMENTAL RESULTS

In this section we describe the properties of the two inelastic reactions and give representative distributions throughout our data. Preliminary analyses of these final states are left until Sec. V.

A. Mass-Squared Distributions

In Fig. 15 we show the Dalitz plots for the two inelastic channels at four energies within our range, while in Figs. 16 and 17 we give the corresponding projections (the origin of the curves in Fig. 16 is discussed in Sec. V). The major features of resonance production are apparent from these plots. At low energies there is copious $\pi\Delta(1238)$ production, Clebsch-Gordan coefficients favoring the production of Δ^- in the $I=\frac{1}{2}$ component of the $\pi^+\pi^- n$ final state,[14] which has large contributions from the $D_{13}(1530)$, $D_{15}(1670)$, and $F_{15}(1680)$ resonances. At higher energies ρN production becomes increasingly important, eventually dominating $\pi\Delta$ production.

At low energies the well-known enhancement at high $\pi\pi$ masses is observed in the $\pi^+\pi^- n$ final state[15] but not in $\pi^-\pi^0 p$. The origin of this effect is complicated and requires a sophisticated analysis for its interpretation.[13]

From approximately 1700 MeV onwards the production of Δ^-, particularly in the backward direction, falls rapidly (see Sec. V) as one might expect in the absence of exotic resonance contribution to the diagrams indicated in Fig. 18.

B. Production Angular Distributions

In Figs. 19 and 20 we show the production angular distributions of the three final-state particles at the same c.m. energies. At lower energies the $\pi\pi N$

TABLE IV. Fractions of resonance and phase-space production in the reaction $\pi^- p \to \pi^+\pi^- n$.

$E_{\text{c.m.}}$ (MeV)	Δ^-	Δ^+	ρ^0	Phase space
1496	0.529 ± 0.087	0.052 ± 0.079	0	0.419 ± 0.118
1527	0.500 ± 0.069	0.187 ± 0.066	0	0.313 ± 0.095
1556	0.565 ± 0.086	0.337 ± 0.082	0	0.098 ± 0.119
1589	0.639 ± 0.056	0.157 ± 0.050	0	0.204 ± 0.075
1629	0.357 ± 0.072	0.017 ± 0.064	0.091 ± 0.049	0.535 ± 0.108
1647	0.551 ± 0.024	0.036 ± 0.020	0.011 ± 0.015	0.402 ± 0.035
1660	0.545 ± 0.035	0.051 ± 0.030	0.003 ± 0.021	0.401 ± 0.045
1669	0.535 ± 0.026	0.025 ± 0.021	0.010 ± 0.016	0.430 ± 0.037
1674	0.537 ± 0.026	0.016 ± 0.021	0.031 ± 0.015	0.416 ± 0.037
1685	0.576 ± 0.027	0.072 ± 0.023	0.003 ± 0.016	0.349 ± 0.039
1695	0.554 ± 0.036	0.006 ± 0.029	0.004 ± 0.020	0.564 ± 0.050
1709	0.440 ± 0.068	0.000 ± 0.052	0.011 ± 0.034	0.451 ± 0.092
1720	0.590 ± 0.064	0.114 ± 0.055	0.000 ± 0.037	0.296 ± 0.092
1730	0.452 ± 0.039	0.001 ± 0.031	0.082 ± 0.025	0.465 ± 0.056
1740	0.569 ± 0.026	0.075 ± 0.020	0.057 ± 0.017	0.299 ± 0.037
1761	0.590 ± 0.043	0.111 ± 0.036	0.097 ± 0.030	0.202 ± 0.064
1762	0.431 ± 0.036	0.096 ± 0.030	0.108 ± 0.025	0.365 ± 0.052
1766	0.348 ± 0.038	0.000 ± 0.028	0.225 ± 0.027	0.427 ± 0.054
1787	0.412 ± 0.044	0.087 ± 0.034	0.173 ± 0.033	0.328 ± 0.065
1806	0.363 ± 0.082	0.056 ± 0.068	0.278 ± 0.071	0.303 ± 0.128
1811	0.330 ± 0.034	0.081 ± 0.028	0.231 ± 0.029	0.358 ± 0.053
1821	0.279 ± 0.034	0.006 ± 0.026	0.293 ± 0.029	0.422 ± 0.053
1843	0.245 ± 0.023	0.045 ± 0.019	0.307 ± 0.029	0.403 ± 0.042
1853	0.250 ± 0.025	0.069 ± 0.022	0.337 ± 0.024	0.344 ± 0.041
1873	0.179 ± 0.020	0.042 ± 0.017	0.364 ± 0.020	0.413 ± 0.033
1884	0.249 ± 0.022	0.030 ± 0.017	0.411 ± 0.022	0.310 ± 0.035
1904	0.184 ± 0.018	0.079 ± 0.017	0.377 ± 0.020	0.360 ± 0.032
1916	0.174 ± 0.016	0.057 ± 0.014	0.424 ± 0.018	0.345 ± 0.028
1932	0.149 ± 0.021	0.061 ± 0.019	0.412 ± 0.024	0.378 ± 0.037
1935	0.154 ± 0.024	0.109 ± 0.023	0.404 ± 0.028	0.333 ± 0.043
1973	0.142 ± 0.014	0.075 ± 0.013	0.426 ± 0.017	0.357 ± 0.026
1980	0.125 ± 0.087	0.087 ± 0.013	0.426 ± 0.017	0.362 ± 0.090

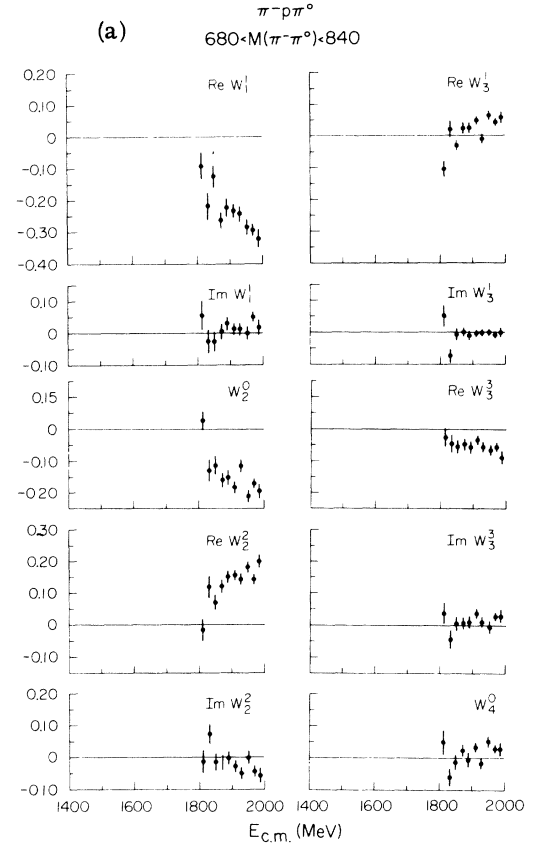

FIG. 28. (a) and (b) The moments W_L^M as a function of energy in the final state $\pi^-\pi^0 p$ for $680 < M(\pi^-\pi^0) < 840$ MeV normalized such that $W_0^0 = 1$ [see Eq. (4′)]. The x axis is defined as $\vec{P}_p$ and the z axis as $\vec{P}_{\pi^-} \times \vec{P}_{\pi^0}$.

system is dominated by the decay of s-channel resonances leading to more symmetrical and isotropic distributions. However as the energy increases a peripheral nature of the reactions begins to emerge as characterized by the production angular distribution of the final nucleon. One other feature worth remarking on is the presence of the forward peak in the π^+ production angular distribution in the $\pi^+\pi^- n$ final state. If interpreted in terms of a t-channel effect (see Fig. 18) this would imply the presence of exotic exchange but it is probably due to the persistence of s-channel contributions. As remarked earlier, the production cross section of the Δ^- is falling rapidly at the higher energies. These data have already been used to indicate an explanation of forward Δ^- production observed in the reaction[16-18]

$$p^+ n \to \Delta^- \pi^+ p.$$

C. Moments Analysis

A complete description of 3-particle final states in terms of angular and mass projections is impossible. A better description, though still not complete, is in terms of moments.[19-22] To do this we express the angular distribution of the incident target proton in a c.m. coordinate system defined by the final-state particles. We write

$$\frac{d\sigma}{d\Omega} = \sum_{L,M} \left(\frac{2L+1}{4\pi}\right)^{1/2} B_L^M Y_L^{M*}(\theta,\phi), \tag{4}$$

where θ and ϕ are the polar coordinates of the in-

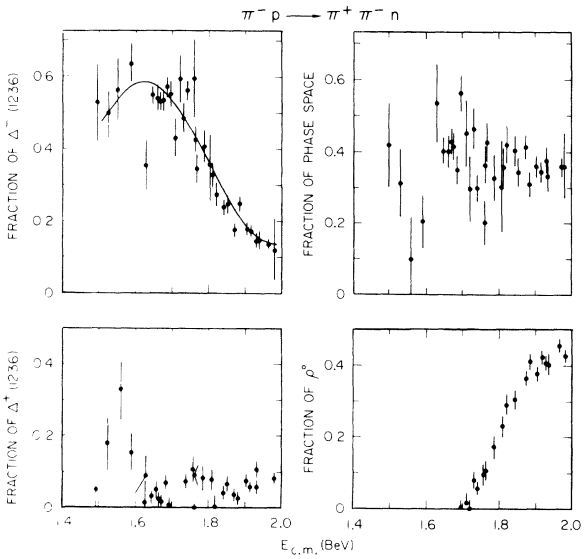

FIG. 29. The fractions of resonance and phase-space production in the reaction $\pi^- p \to \pi^-\pi^+ n$.

cident proton. Equation (4) can be rewritten as

$$\frac{1}{\sigma}\frac{d\sigma}{d\Omega} = \frac{1}{4\pi} + \sum_{L\geq 1}\sum_{M}\left(\frac{2L+1}{4\pi}\right)^{1/2}\frac{B_L^M}{B_0^0}\,Y_L^{M*}(\theta,\phi)$$

$$= \frac{1}{4\pi} + \sum_{L\geq 1}\sum_{M}\left(\frac{2L+1}{4\pi}\right)^{1/2} W_L^M Y_L^{M*}(\theta,\phi), \quad (4')$$

i.e., W_0^0 is normalized to unity.

In order to give a useful representation of the data we have calculated the moments W_L^M for the following categories of events as a function of energy:

(i) all data,

(ii) events lying within

$1.140 < M(\pi^-n) < 1.320$ BeV $(\pi^+\pi^-n)$,

$1.140 < M(\pi^-p) < 1.320$ BeV $(\pi^-p\pi^0)$;

(iii) events lying within

$1.140 < M(\pi^+n) < 1.320$ BeV $(\pi^+\pi^-n)$,

$1.140 < M(\pi^0p) < 1.320$ BeV $(\pi^-p\pi^0)$;

(iv) events lying within

$0.680 < M(\pi^+\pi^-) < 0.840$ BeV $(\pi^+\pi^-n)$,

$0.680 < M(\pi^-\pi^0) < 0.840$ BeV $(\pi^-p\pi^0)$,

So that the angular distributions are suitable for comparison with models for the production of Δ and ρ resonances we have used a variety of coordinate systems. In all cases we have taken the normal to the final 3-particle plane as the OZ axis

$OZ = \vec{P}_{\pi^-} \times \vec{P}_{\pi^+}$ $(\pi^+\pi^-n)$,

$OZ = \vec{P}_{\pi^-} \times \vec{P}_{\pi^0}$ $(\pi^-p\pi^0)$,

but the definition of OX changes. These definitions are

(i) and (iv) $OX = \vec{P}_N$;

(ii) $OX = \vec{P}_{\pi^+}$ $(\pi^+\pi^-n)$,

$OX = \vec{P}_{\pi^0}$ $(\pi^-p\pi^0)$;

(iii) $OX = \vec{P}_{\pi^-}$ $(\pi^+\pi^-n)$,

$OX = \vec{P}_{\pi^-}$ $(\pi^-p\pi^0)$.

The axis OY is then given by

$$OY = OZ \times OX.$$

$\vec{P}_N$, $\vec{P}_{\pi^-}$, and $\vec{P}_\pi$ are the momenta of the three final-state particles measured in the c.m. system.

Parity conservation[21,22] implies that

$W_L^M = 0$ if $L+M$ is odd.

Interference waves of the same parity contribute to those W_L^M with L even, while interference of waves of opposite parity only give W_L^M with L odd.[21,22]

In Figs. 21–28 we give the variation of these moments for $L \leq 5$ throughout the range of our data.[23] The data are available in tabular form elsewhere.[24] Moments for $L > 5$ are consistent with zero as are those moments forbidden by parity conservation.

A wave of total angular momentum j contributes to terms with $L \leq 2j-1$. In the region of ~1700 MeV $L=4$ moments are nonzero due to the presence of the D_{15} and F_{15} resonances. However $L=5$ moments, corresponding to the interference effects of these resonances, are consistent with zero indicating the presence of cancellations in the Dalitz plot. Even at the highest energies these moments indicate that only waves of $j \leq \frac{5}{2}$ are necessary, but one should be careful in light of the cancellations we know can occur.

The structure in W_1^1 in the region of 1500 MeV we presume is due to interference between P_{11} and D_{13} resonances. Indeed the large values of moments with L odd indicate the presence of appreciable quantities of waves of opposite parities at all c.m. energies.

V. INTERPRETATION AND ANALYSIS OF THE DISTRIBUTIONS

Two preliminary analyses of the data have been made: (i) an analysis of the Dalitz plot in the $\pi^-\pi^+n$ final state; (ii) a partial-wave analysis of a subsample of events comprising the reaction

$$\pi^- p \to \pi^+\Delta^-$$

in the region of the F_{15} and D_{15} resonances. This latter analysis has been presented elsewhere.[25]

A. Analysis of the Dalitz plot in $\pi^+\pi^-n$

The Dalitz plot has been fitted using the maximum-likelihood fitting program MURTLEBURT.[26] This uses an incoherent sum of processes to describe the reaction, the processes in this case being

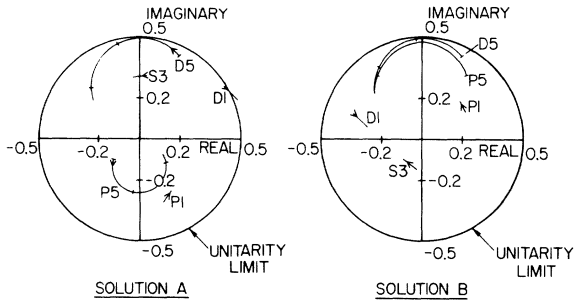

FIG. 30. Variation of the partial-wave amplitudes in two solutions A and B, resulting from fits (Ref. 21) to the reaction $\pi^- p \to \pi^+\Delta^-$. Tick marks correspond to the c.m. energies 1647, 1685, and 1740 MeV.

TABLE V. F_{15} and D_{15} resonance parameters from a partial-wave analysis of the reaction $\pi^- p \to \Delta^- \pi^+$.

Resonance	Parameter	Solution *A*	Solution *B*
F_{15}	Mass	1.690 ± 0.005	1.686 ± 0.009
	Width	0.077 ± 0.022	$0.130^{+0.035}_{-0.053}$
	$\Delta\pi$ branching fraction	$0.13^{+0.03}_{-0.04}$	$0.39^{+0.06}_{-0.10}$
D_{15}	Mass	1.671 ± 0.004	1.680 ± 0.009
	Width	0.112 ± 0.017	$0.158^{+0.090}_{-0.020}$
	$\Delta\pi$ branching fraction	0.63 ± 0.07	$0.63^{+0.07}_{-0.11}$
Relative sign of D_{15} and F_{15} coupling to $\Delta\pi$		$-$	$+$

$\pi^- p \to \pi^+ \Delta^-$

$\to \pi^- \Delta^+$

$\to \rho^0 n$ (only above a c.m. energy of 1600 MeV)

$\to \pi^+ \pi^- n$ phase space.

The resonance amplitudes are written in the form of a relativistic Breit-Wigner[27]

$$T = \Gamma_0 \omega_0 \left(\frac{\omega}{\omega_0}\right)\left(\frac{q_0}{q}\right) \frac{\omega_0 \Gamma(\omega)}{(\omega_0^2 - \omega^2) + \omega_0^2 \Gamma^2(\omega)} \cdots, \qquad (5)$$

where

$$\Gamma(\omega) = \Gamma_0 \left(\frac{q}{q_0}\right)^{2L+1} \frac{B_L(qr)}{B_L(q_0 r)}$$

and

ω = diparticle mass,

q = momentum in diparticle decay,

ω_0 = resonance mass,

q_0 = momentum of particles when $\omega = \omega_0$,

Γ_0 = width of the resonance at $\omega = \omega_0$,

Γ = decay width at mass ω,

$B_L(qr)$ = barrier penetration factor,[28]

L = orbital angular momentum in the decay of the resonance.

The factors present in (5) normalize the amplitude at resonance to unity. We use the following values for the masses and widths of the resonances in the fit.

$M(\Delta) = 1236$ MeV, $\Gamma_0(\Delta) = 130$ MeV,

$M(\rho) = 765$ MeV, $\Gamma_0(\rho) = 130$ MeV.

The fractions of the various resonance and phase-space contributions determined by this method are given in Table IV and Fig. 29. The quality of the fits can be seen by inspecting Fig. 16 where the curves are derived from the final fits. Below a c.m. energy of 1496 MeV no fits were obtained due to the large overlap of the Δ bands in the Dalitz plot. The steady decrease in the fraction of Δ^- is apparent together with the rapid increase in ρ^0 production from threshold.

A similar attempt to fit the $\pi^- \pi^0 p$ final state was inconclusive, presumably because the incoherent sum of the amplitudes for the various processes cannot describe the final state.

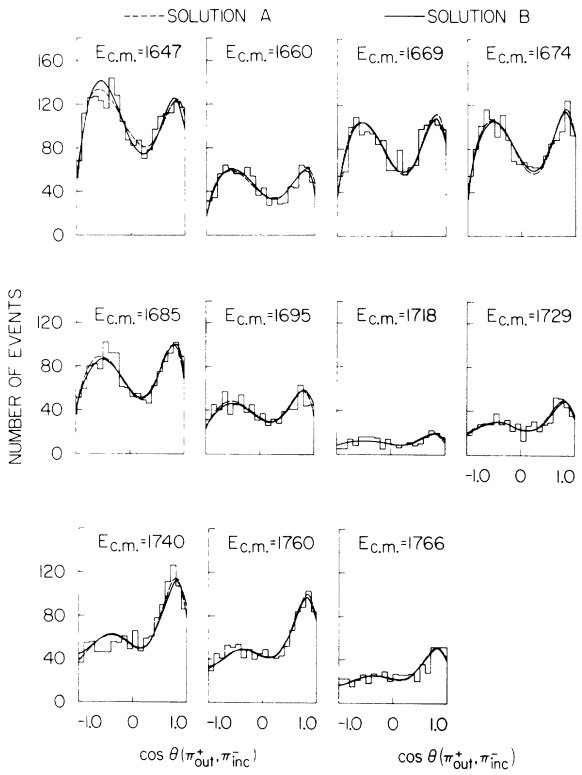

FIG. 31. Fits to the production angular distributions of the π^+ in the reaction $\pi^- p \to \pi^+ \Delta^-$ in solutions *A* and *B*.[21]

B. Partial-wave analysis of $\pi^- p \to \pi^+ \Delta^-$ in the c.m. energy range 1647-1766 MeV

The analysis of this reaction has been described elsewhere[25] and we present only a summary of the conclusions here.

The production angular distribution and cross sections for the reaction were fitted using the partial-wave analysis described by Brody and Kernan.[29] The partial-wave amplitudes used were (the notation employed is L, $2J$ where L is the $\pi\Delta$ orbital angular momentum and J the total angular momentum)

(1) $P5$ containing the F_{15} resonance,
$D5$ containing the D_{15} resonance,

(2) $S3$, $P1$, $D1$, and $F7$ containing background amplitudes.

The resonances are described by Breit-Wigner shapes and the backgrounds are parametrized as linear functions of the c.m. momentum.

In the analysis two solutions, A and B, were found. The F_{15} and D_{15} resonance parameters corresponding to these solutions are given in Table V, while the variations of the resonant amplitudes and the background amplitudes are shown in Fig. 30. In Fig. 31 we display the fits to the production angular distributions at all energy points in our analysis and in Fig. 32 we give the contributions of the individual waves to the cross section.

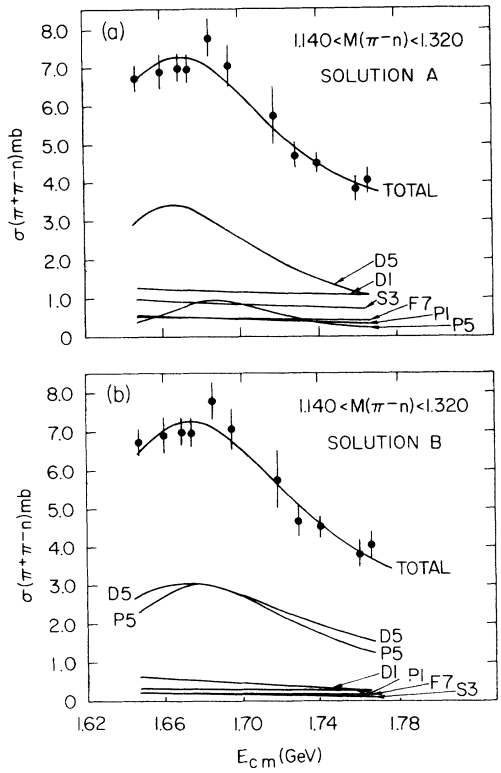

FIG. 32. The experimental $\pi^+\pi^-n$ cross section [1140 $< M(\pi^-n) <$ 1320 MeV] together with the contributions of the various partial waves in solution A and B.[21]

VI. DISCUSSION OF RESULTS

The interpretation of the single-pion production data is exceedingly complicated. The analyses described here are only a beginning and more sophisticated approaches are required.[13,21,22] At present we are pursuing an analysis (within the spirt of isobar model) using a maximum-likelihood fit to the data. Such analyses require large quantities of time and we felt it worthwhile to present the experimental data at an earlier stage. Only when this analysis is complete will we begin to have a description of the $\pi\pi N$ final state.

However, even the experimental presentation of 3-body final states presents many problems which we do not pretend to have surmounted. In the future we hope to have available magnetic tapes containing the experimental information, this being the only solution to these problems.

VII. ACKNOWLEDGMENTS

We would like to thank F. S. Crawford Jr. and J. A. Anderson for making available the LRL HBC film. We also wish to thank the LRL Spiral Reader crew and especially G. R. Lynch and L. J. Lloyd for their help and assistance in measuring the film, and the SLAC CDA staff for their scanning effort. Finally, we wish to acknowledge the valuable assistance at the early stage of the experiment of R. Diebold.

---

*Work supported by the U. S. Atomic Energy Commission.

†Present address is CERN, Geneva, Switzerland.

‡Present address is University of California, Riverside, California.

§Present address is Dept. de Physique des Particules Elementaires, CEN, Saclay, France.

‖Present address is University of California, Irvine, California.

**Present address is DESY, Hamburg, Germany.

[1] P. Bareyre, C. Bricman, A. V. Stirling, and G. Villet, Phys. Letters 18, 342 (1965); P. Bareyre, C. Bricman, and G. Villet, Phys. Rev. 165, 1730 (1968).

[2] B. H. Bransden, P. J. O'Donnell, and R. G. Moorhouse, Phys. Letters 11, 339 (1964); Phys. Rev. 139, B1566 (1965); Proc. Roy. Soc. (London) A289, 538 (1966); Phys.

Letters 19, 420 (1965).
[3]P. Auvil, A. Donnachie, A. T. Lea, and C. Lovelace, Phys. Letters 12, 76 (1964); 19, 148 (1965).
[4]L. D. Roper, Phys. Rev. Letters 12, 340 (1964); L. D. Roper, R. M. Wright, and B. T. Feld, Phys. Rev. 138, B190 (1965); L. D. Roper and R. M. Wright *ibid.* 138, B921 (1965).
[5]R. J. Cence, Phys. Letters 20, 306 (1966).
[6]C. H. Johnson, Lawrence Radiation Laboratory Report No. UCRL-17683, 1967 (unpublished).
[7]A. Donnachie, R. G. Kirsopp, and C. Lovelace, Phys. Letters 26B, 161 (1968); C. Lovelace, in *Proceedings of the International Conference on Elementary Particles, Heidelberg, Germany, 1967,* edited by H. Filthuth (North-Holland, Amsterdam, 1967), p. 79; C. Lovelace in *Proceedings of the Conference on πN Scattering, Irvine, California, 1967,* edited by G. L. Shaw and D. Y. Wong (Wiley, New York, 1967); CERN Report No. CERN-TH-839, 1967 (unpublished).
[8]R. G. Moorhouse, Ann. Rev. Nucl. Sci. 19, 301 (1969).
[9]R. J. Plano, in *Proceedings of the Lund International Conference on Elementary Particles,* edited by G. von Dardel (Berlingska, Lund, Sweden, 1970), p. 313.
[10]A. D. Brody, R. J. Cashmore, A. Kernan, D. W. G. S. Leith, B. S. Levi, B. C. Shen, J. P. Berge, D. J. Herndon, L. R. Price, A. H. Rosenfeld, and P. Söding, Phys. Rev. D 3, 2619 (1971).
[11]Due to variations in the reliability of the pulse-height information from the Spiral Reader it is necessary, in constructing $\chi_{\text{comb}}{}^2$, to introduce a factor α which reflects this fact. Thus we used $\chi_{\text{comb}}{}^2 = \chi_K{}^2 + \alpha\chi_{\text{ion}}{}^2$, where $\alpha = 2.0/\langle\chi_{\text{ion}}{}^2\rangle$ and $\langle\chi_{\text{ion}}{}^2\rangle$ was determined from 100 unambiguous inelastic events at a time. α varied from 0.8 to 0.25.
[12]A. A. Carter, K. F. Riley, R. J. Tapper, D. V. Bugg, R. S. Gilmore, K. M, Knight, D. C. Salter, G. H. Stafford, E. J. N. Wilson, J. D. Davies, J. D. Dowell, P. M. Hattersley, R. J. Homer, and A. W. O'Dell, Phys. Rev. 168, 1457 (1968).
[13]M. De Beer, B. Deler, J. Dolbeau, M. Neveu, Nguyen Thuc Diem, G. Smadja, and G. Valladas, Nucl. Phys. B12, 599 (1969); W. Chinowsky, J. H. Mulvey, and D. H. Saxon, Phys. Rev. D 2, 1790 (1970).
[14]$\pi\Delta$ production in different isospin states leads to the following ratios (neglecting any interference effects):

$$I=\tfrac{1}{2}: \pi^+\pi^-n,\ \frac{\Delta^-}{\Delta^+}=\frac{9}{1};\quad \pi^-\pi^0p,\ \frac{\Delta^0}{\Delta^+}=\frac{2}{2};\quad \frac{\pi^+\pi^-n}{\pi^-\pi^0p}=\frac{10}{4}.$$

$$I=\tfrac{3}{2}: \pi^+\pi^-n,\ \frac{\Delta^-}{\Delta^+}=\frac{18}{8};\quad \pi^-\pi^0p,\ \frac{\Delta^0}{\Delta^+}=\frac{1}{16};\quad \frac{\pi^+\pi^-n}{\pi^-\pi^0p}=\frac{26}{17}.$$

ρN production in different isospin states leads to the following ratios:

$$I=\tfrac{1}{2}: \frac{\pi^+\pi^-n}{\pi^-\pi^0p}=\frac{1}{2};$$

$$I=\tfrac{3}{2}: \frac{\pi^+\pi^-n}{\pi^-\pi^0p}=\frac{2}{1}.$$

[15]J. Kirz, J. Schwarz, and R. D. Tripp, Phys. Rev. 130, 2481 (1963); C. N. Vittitoe, B. R. Riley, W. J. Fickinger, V. P. Kenney, J. G. Mowat, and W. D. Shephard, Phys. Rev. 135, 232 (1964).
[16]H. O. Cohn, R. D. McCulloch, W. M. Bugg, and G. T. Conde, Phys. Letters 26B, 598 (1969).
[17]G. Yekutieli, D. Yaffe, S. Toaff, A. Shapira, E. E. Ronat, U. Karson, B. Haber, and Y. Eisenberg, Phys. Rev. Letters 25, 184 (1970).
[18]E. L. Berger and R. A. Morrow, Phys. Rev. Letters 25, 1136 (1970).
[19]D. Branson, P. V. Landshoff, and J. C. Taylor, Phys. Rev. 132, 902 (1963).
[20]R. C. Arnold and J. L. Uretsky, Phys. Rev. 153, 1443 (1967).
[21]D. H. Morgan, Phys. Rev. 166, 1731 (1968).
[22]R. J. Cashmore, Ph.D. thesis, Oxford University, England (unpublished).
[23]We only give moments for $M \geq 0$. Other values may be obtained using the relation $W_L^{-M} = (-1)^M W_L^{M*}$.
[24]A. D. Brody, R. J. Cashmore, A. Kernan, D. W. G. S. Leith, B. G. Levi, A. Minten, B. C. Shen, J. P. Berge, B. Deler, D. J. Herndon, R. Longacre, L. R. Miller, L. R. Price, A. Rosenfeld, and P. Söding, SLAC Report No. SLAC-PUB-911, Suppl. 1 (unpublished).
[25]A. D. Brody, R. J. Cashmore, A. Kernan, D. W. G. S. Leith, B. G. Levi, B. C. Shen, D. J. Herndon, L. R. Price, A. H. Rosenfeld, and P. Söding, Phys. Letters 34B, 665 (1971).
[26]MURTLEBURT, J. Friedman, Lawrence Radiation Laboratory, Alvarez Programming Group Note No. P-156 (unpublished).
[27]J. D. Jackson, Nuovo Cimento 34, 1644 (1964).
[28]J. M. Blatt and V. F. Weisskopf, *Theoretical Nuclear Physics* (Wiley, New York, 1956).
[29]A. D. Brody and A. Kernan, Phys. Rev. 182, 1785 (1969).

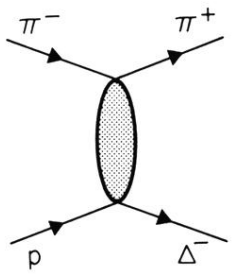

FIG. 18. Diagram for the production of forward π^+ mesons in the reaction $\pi^- p \to \pi^+ \Delta^-$.

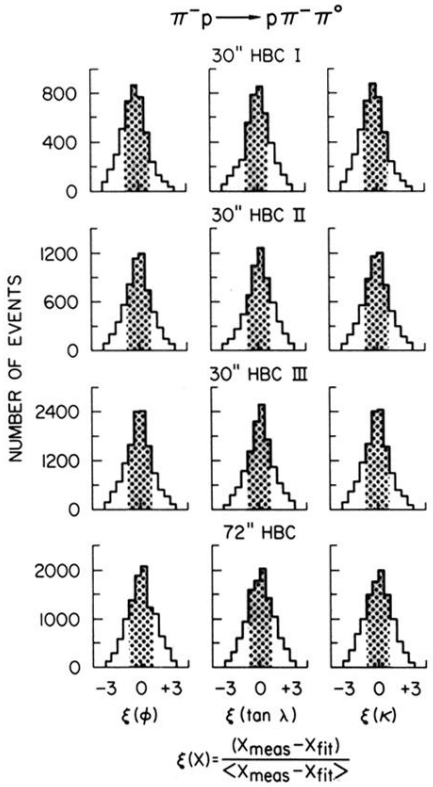

FIG. 2. Beam-track pull quantities in the reaction $\pi^- p \rightarrow \pi^-\pi^0 p$. The shaded area corresponds to ± 1. For definitions of HBC I, HBC II, and HBC III, see Table I.